Phospholamban and Its Phosphorylated Form Interact Differently with Lipid Bilayers: A ^{31}P, ^{2}H, and ^{13}C Solid-State NMR Spectroscopic Study†

Shadi Abu-Baker and Gary A. Lorigan*

Department of Chemistry and Biochemistry, Miami University, Oxford, Ohio 45056

Received July 12, 2006; Revised Manuscript Received August 30, 2006

ABSTRACT: Phospholamban (PLB) is a 52-amino acid integral membrane protein that helps to regulate the flow of Ca^{2+} ions in cardiac muscle cells. Recent structural studies on the PLB pentamer and the functionally active monomer (AFA-PLB) debate whether its cytoplasmic domain, in either the phosphorylated or dephosphorylated states, is α-helical in structure as well as whether it associates with the lipid head groups (Oxenoid, K. (2005) *Proc. Natl. Acad. Sci. U.S.A. 102*, 10870−10875; Karim, C. B. (2004) *Proc. Natl. Acad. Sci. U.S.A. 101*, 14437−14442; Andronesi, C.A. (2005) *J. Am. Chem. Soc. 127*, 12965−12974; Li, J. (2003) *Biochemistry 42*, 10674−10682; Metcalfe, E. E. (2005) *Biochemistry 44*, 4386−4396: Clayton, J. C. (2005) *Biochemistry 44*, 17016−17026). Comparing the secondary structure of the PLB pentamer and its phosphorylated form (P-PLB) as well as their interaction with the lipid bilayer is crucial in order to understand its regulatory function. Therefore, in this study, the full-length wild-type (WT) PLB and P-PLB were incorporated into 1-palmitoyl-2-oleoyl-sn-glycero-phosphocholine (POPC) phospholipid bilayers and studied utilizing solid-state NMR spectroscopy. The analysis of the ^{2}H and ^{31}P solid-state NMR data of PLB and P-PLB in POPC multilamellar vesicles (MLVs) indicates that a direct interaction takes place between both proteins and the phospholipid head groups. However, the interaction of P-PLB with POPC bilayers was less significant compared that with PLB. Moreover, the secondary structure using $^{13}C{=}O$ site-specific isotopically labeled Ala15-PLB and Ala15-P-PLB in POPC bilayers suggests that this residue, located in the cytoplasmic domain, is a part of an α-helical structure for both PLB and P-PLB.

High-resolution solution NMR[1] techniques are commonly used to probe the structure of proteins and peptides in solution and micelles (*1*−*10*). Membrane proteins inserted into synthetic phospholipid bilayers mimic the biological membrane environment better than micelles (*11*−*15*). Alternatively, solid-state NMR spectroscopy is routinely used to determine the structural and dynamic properties of both membrane macromolecules and peptides in phospholipid bilayers (*16*−*22*). From the perspective of the lipids, ^{2}H solid-state NMR spectroscopy can be used to probe the possible orientation and dynamics of peptides or proteins incorporated into deuterated phospholipid bilayers (*23*−*28*). Moreover, ^{31}P solid-state NMR spectroscopy can be used to investigate the interaction of peptides, proteins, and drugs with phospholipid head groups (*26*−*29*). The secondary structure of $^{13}C{=}O$ site-specific isotopically labeled peptides or proteins inserted into lipid bilayers can be probed utilizing ^{13}C CPMAS solid-state NMR spectroscopy (*30*−*33*).

Phospholamban (PLB) is a 52-amino acid transmembrane protein that interacts with the Ca-ATPase pump and lowers its affinity for Ca^{2+} (*34*−*36*). PLB plays a major role in the regulation process of the cardiac cycle (includes both contraction and relaxation), which controls the heartbeat (*36*−*38*). Unphosphorylated PLB inhibits sacroplasmic reticulum ATPase activity and stops the flow of Ca^{2+} ions, and this inhibition can be relieved by the cyclic AMP- and calmodulin-dependent phosphorylation of PLB (*36*−*38*). Heart failure can be induced by abnormal relaxation of cardiac muscle cells, possibly caused by disproportionate ratios of Ca^{2+}-ATPase and PLB in heart muscle cells leading to abnormal levels of Ca^{2+} ions as observed in failed human and animal hearts (*39*). Because PLB is biologically significant and it is relatively small in size, many theoretical and biophysical experimental studies have been conducted to investigate its structure in a membrane (*40*−*56*). Fuji and co-workers elucidated the complete PLB primary structure by amino acid sequencing (*43*). Also, they reported that the molecular mass of the PLB monomer is about 6 kD and

† This work was supported by AHA Scientist Development Grant 0130396N, NIH Grant GM60259-01, and NSF CAREER Award CHE-0133433. The 500 MHz wide bore NMR spectrometer was obtained from NSF Grant 10116333.

* To whom correspondence should be addressed. Phone: 513-529-3338. Fax: 513-529-5715. E-mail: garylorigan@muohio.edu.

[1] Abbreviations: P-PLB, phosphorylated phospholamban; PLB, phospholamban; TM-PLB, the transmembrane domain of phospholamban; AFA-PLB, the monomeric mutated form of PLB; SERCA, sarco-(endo)plasmic reticulum calcium ATPase; MLVs, multilamellar vesicles; POPC, 1-palmitoyl-2-oleoyl-sn-glycero-phosphocholine; POPC-d_{31}, deuterated POPC (*sn*-1 chain); S_{CD}, molecular order parameters; CSA, chemical shift anisotropy; HCL, hydrochloric acid; TFE, 2,2,2-triflouroethanol; NMR, nuclear magnetic resonance; CPMAS, cross-polarization magic-angle spinning; HPLC, high performance liquid chromatography; IPA, isopropanol; MeCN, acetonitrile; TMS, tetramethylsilane; MALDI-TOF, matrix assisted laser desorption ionization time-of-flight mass spectrometry; SDS−PAGE, sodium dodecyl (lauryl) sulfate−polyacrylamide gel electrophoresis.

10.1021/bi0614028 CCC: $33.50
Published on Web 10/17/2006

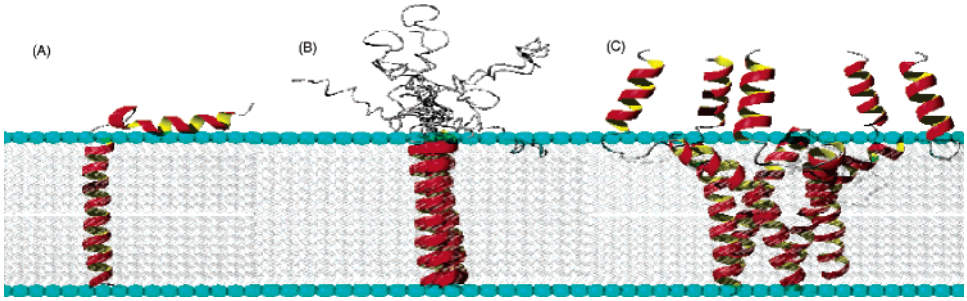

FIGURE 1: Proposed structural models of pentameric and monomeric phospholamban in a lipid bilayer. (A) L-shaped monomeric NMR solution structure of AFA-PLB by the Veglia group (*60*). (B) Solid-state NMR monomeric structure of AFA-PLB by the Baldus group (*57*). (C) NMR solution structure of pentameric PLB by the Chou group (*61*). This figure was generated using the MOLMOL software and a G5 Apple Mac computer (*94*). The 3D structures in A, B, and C were obtained from the published reports and the Protein Data Bank.

determined that PLB is a pentamer consisting of five identical subunits (*43*). The functional form of PLB is believed to consist of a homopentameric cluster, which retains activity when reconstituted into lipid bilayers (*40*, *48*).

Early structural studies on PLB disagreed on the structure of PLB embedded in lipid membranes (*42*, *55*). In one structural model suggested by Arkin and co-workers, a continuous α-helix with a tilt angle of approximately 28° for PLB with respect to the bilayer normal has been proposed (*42*). In another model suggested by Tatulian and co-workers, PLB is composed of two α-helices connected by an unstructured/*β*-sheet region with a cytoplasmic domain tilted in a range of 50−60° with respect to the bilayer normal (*55*). The earlier two structural models of PLB were based upon spectroscopic studies and molecular modeling techniques for pentameric PLB (*42*, *55*).

Recently, new high-resolution solution NMR studies as well as other structural techniques have been used to describe the orientation and dynamics of the functionally active AFA-PLB monomer and PLB pentamer (*57*−*61*). First, an L-shaped model has been proposed for the AFA-PLB mutant by the Veglia group utilizing ^{15}N solid-state NMR spectroscopy (*59*). Also, the same group reported a high-resolution solution NMR structure of the monomeric AFA-PLB mutant (illustrated in Figure 1A) (*60*). Their data indicates that AFA-PLB has an L-shape structure, and the cytosolic segment of AFA-PLB lies directly on the membrane surface (*59*, *60*). Another model for AFA-PLB proposed by the Baldus group, indicates a non-α-helical disordered cytosolic domain model for the monomer utilizing cross-polarization magic angle spinning (CPMAS) solid-state NMR spectroscopy (Figure 1B) (*57*). Finally, the Chou group reveals an unusual bellflower-like assembly for pentameric WT-PLB in micelles utilizing high-resolution solution NMR spectroscopy (*61*). This channel-like architecture holds the monomers together by leucine/isoleucine zipper motifs (*61*). The central pore of the twisted transmembrane helices widens gradually toward the cytoplasmic end (*61*). Chou's high-resolution solution NMR structure of WT-PLB is illustrated in Figure 1C, and it indicates that the relatively mobile cytoplasmic domain of the pentamer on average points away from the membrane surface (*61*). Alternatively, the results from the Middleton group suggest that the cytoplasmic domain of PLB (residues 1−23) is stabilized through its association with the phospholipid bilayer surface (*62*).

The transmembrane segment for all three structures illustrated in Figure 1A, B, and C is α-helical. However, the structure of the cytoplasmic domain differs significantly. In both the L-shaped and the bellflower-like assembly solution NMR structures, the cytoplasmic domain is α-helical (*59*, *61*). The Baldus model suggests that the cytoplasmic domain of AFA-PLB is not α-helical (*57*). Additionally, while the L-shaped high-resolution solution NMR structure and the Middleton group studies suggest that the cytoplasmic domain interacts with the membrane surface (*58*, *59*, *62*), the Chou and the Baldus structures suggest that the cytoplasmic domain has minimal interactions with the membrane surface (phospholipid head groups) (*57*, *61*). Therefore, PLB's cytoplasmic segment secondary structure, orientation, dynamics, and interaction with the membrane are clearly under serious debate.

Similarly, the effect of phosphorylation on the cytoplasmic domain is also not well understood. Although the Chou group did not resolve the solution structure of P-PLB, they hypothesized that introducing a negative charge upon phosphorylation of PLB could alter the average orientation of the cytoplasmic domain and decrease its accessibility to the calcium pump (*61*). Previously, Veglia indicated that phosphorylation of serine 16 (located within the cytoplasmic domain) of the AFA-PLB monomer induces an order-to-disorder transition that disrupts the L-shaped AFA-PLB and causes a reduction in the α-helical secondary structure around the phosphorylation site (*63*). This finding contradicts an older report by Bigelow and co-workers, which suggested that the phosphorylation of AFA-PLB increases the stabilization of the helical content, especially in the hinge region, leaving the cytoplasmic domain associated with the membrane (*63*, *64*).

Three models have been proposed to describe PLB interacting with sarco(endo)plasmic reticulum calcium ATPase (SERCA) (*36*, *61*, *65*). In the first and earliest model, the dephosphorylated pentamer dissociates to a PLB monomer that inhibits sacroplasmic reticulum ATPase activity by binding to the cytoplasmic and transmembrane domains of the calcium pump. Phosphorylation of PLB at Ser 16 or Thr 17 reduces its electrostatic binding with the pump (*34*, *36*). Consequently, the calcium pump inhibition will be reversed, and the association of PLB monomers into pentamers is favored (*36*).

In the second model, an allosteric interaction between the PLB monomer and SERCA takes place (*65*). When PLB is in its free form (not interacting with SERCA), the monomer interconverts between the bent form (T-state, inactive, highly ordered L-shape, cytoplasmic domain facing the lipids,

predominant) and the extended form (R-state, active, more dynamically disordered with higher affinity to SERCA) (*65*). In the presence of SERCA, the preexisting equilibrium between the two forms is disturbed. The bent form inhibits SERCA because of protein−protein interactions between the transmembrane regions of PLB and SERCA (*65*). Only in the extended form, in which both the cytoplasmic domain and the transmembrane domain of PLB binds to SERCA, the SERCA-PLB complex is capable of reversing SERCA inhibition because of phosphorylation or mutation (*65*, *66*).

In the third and latest model, the tightness of the PLB pentamer (supercoiled Leu/Ile zipper) raises the question of how valuable monomeric PLB is for association with SERCA (*61*). This model suggests that the relatively mobile cytoplasmic domain of the pentamer, which on average points away from the membrane surface, possibly fits into the groove of the SERCA cytoplasmic domain (*61*). On the basis of the suggested PLB channel-like architecture, PLB could function as an ion channel besides its ability to regulate sacroplasmic reticulum ATPase activity (*61*).

Finally, it is important to emphasize that the high-resolution NMR solution structures of the monomeric PLB mutant (AFA-PLB) and the pentameric WT-PLB in micelles reported by the Veglia and Chou groups, respectively, represent two of the best and widely accepted membrane protein structures available in the literature (*60*, *61*). Additionally, EPR spectroscopic studies from the Veglia and Thomas groups indicate that a two-state dynamic equilibrium exists for the cytosolic segment of AFA-PLB in a lipid bilayer (*58*, *65*, *66*). Similarly, the Chou group suggested that their structure of PLB in micelles sets the stage for a series of future experiments to characterize the effect of phosphorylation on the orientation and dynamics of its cytoplasmic helix (*61*). Therefore, in the present study, the full-length pentameric WT-PLB and its phosphorylated form (P-PLB) were used to compare the structural changes in the acyl chains of POPC multilamellar vesicles (MLVs) upon the insertion of both proteins utilizing ^{31}P and ^{2}H solid-state NMR spectroscopy. Additionally, $^{13}C{=}O$ site-specific studies of PLB and P-PLB incorporated into lipid bilayers were used to compare the secondary structure of both PLB forms around the phosphorylation site (Ser16) utilizing ^{13}C CPMAS solid-state NMR spectroscopy.

MATERIALS AND METHODS

Materials. POPC and POPC-d_{31} were purchased from Avanti Polar Lipids (Alabaster, AL). Prior to use, phospholipids were dissolved in chloroform and stored at −20 °C. Chloroform, hexafluoro-2-propanol, formic acid, and 2,2,2 triflouroethanol (TFE) were purchased from Aldrich Chemical Co. (St. Louis, MO). HPLC-grade acetonitrile and 2-propanol were obtained from Pharmco (Brookfield, CT) and were filtered through a 0.2 μm nylon membrane before use. Water was purified using a nanopure reverse osmosis system (Millipore, Bedford, MA). Fmoc-amino acids, prephosphorylated Fmoc-serine amino acid, and other chemicals for peptide synthesis were purchased from Applied Biosystems, Inc. (Fostercity, CA). $^{13}C{=}O$ labeled Leu and Ala Fmoc-amino acids were purchased from Isotec/Sigma-Aldrich (St. Louis, MO). *N*-[2-hydroxyethyl]piperazine-*N*′-2-ethane sulfonic acid (HEPES) and EDTA were obtained from Sigma-Aldrich (St. Louis, MO).

Synthesis and Purification of PLB. The isolation and purification of large quantities of native PLB through molecular biology techniques has not yet been achieved because of difficulties encountered in the bacterial overexpression of phospholamban cDNA (*67*, *68*). Alternatively, PLB has been prepared by chemical synthesis using standard solid-phase peptide synthesis and purification in organic solvents (*69*, *70*). In addition, this approach gives the opportunity to synthesize site-specific isotopically labeled peptides and proteins (*30*, *59*, *71*). The biochemical and biophysical comparison of synthetic PLB and native PLB revealed that they are both similar in size and functionally identical (*69*, *70*). The chemically synthesized form of the full length PLB and P-PLB were used in all of the solid-state NMR experiments presented. PLB was synthesized according to a new procedure developed in our lab. Briefly, PLB was synthesized using modified Fmoc-based solid-phase methods with an ABI 433A peptide synthesizer (Applied Biosystems, Foster city, CA). PLB is very hydrophobic; thus, the synthesis of this peptide is very challenging (see the Supporting Information for more details). In addition, during our first run, we found that the coupling of Leu-7 to Thr-8 was difficult even after double coupling and extending the reaction time to 6 h. However, this problem was solved by using the pseudoproline dipeptide of Fmoc-Leu-Thr ($\Psi^{Me,Me}$ Pro)-OH from Novabiochem (San Diego, CA) (*72*). The use of a pseudoproline dipeptide of Fmoc-Leu-Thr ($\Psi^{Me,Me}$ Pro)-OH enhanced the yield to about 25% after lyophylization. To synthesize P-PLB, a pre-phosphorylated Fmoc-serine amino acid was used at amino acid position 16 instead of the regular Fmoc-serine used in the synthesis of PLB (*73*). Additionally, $^{13}C{=}O$ labeled Leu and Ala amino acids from Isotec/Sigma-Aldrich (St. Louis, MO) were used to synthesize the $^{13}C{=}O$ site-specific isotopically labeled Leu39-PLB, Ala15-PLB and Ala15-P-PLB.

The crude peptide was purified on an Amersham Pharmacia Biotech AKTA explorer 10S HPLC controlled by Unicorn (version 3) system software (see the Supporting Information for more details). The purified protein was lyophilized and characterized by matrix-assisted laser desorption ionization time-of-flight (MALDI-TOF) mass spectrometry and SDS−PAGE (data not shown).

The oligomerization state of WT-PLB and P-PLB was explored using SDS−PAGE analysis (data not shown). Our results are comparable to those of Simmerman and coworkers and indicate that the two peptides are mainly pentameric and did not show the coexistence of any additional dimer bands as reported in the Middleton study on the PLB mutant (*74*, *75*). Additionally, the Smith group has demonstrated with solid-state NMR spectroscopy that the full-length WT-PLB forms a pentamer in PC membranes, and a similar conclusion was reported in our previous TM-PLB study (*71*, *76*).

NMR Sample Preparation. POPC bilayers containing various mol % of P-PLB or PLB in phospholipid were prepared according to the protocol given by Rigby and coworkers (*12*). POPC (35 mg) and PLB or P-PLB were dissolved in $CHCl_3$ and TFE, respectively, and placed into a 12 × 75 mm test tube. The solvents were removed under a steady stream of N_2 gas and then the test tube was placed in vacuum desiccators overnight to remove any residual solvent. The P-PLB/lipid or PLB/lipid mixture was then

resuspended in 95 μL of HEPES buffer (5 mM EDTA, 20 mM NaCl, and 30 mM HEPES at pH 7.0). Finally, after the phospholipids were fully dissolved, the sample was transferred to an NMR sample tube. POPC-d_{31} (8 mg) was added to the samples when conducting the ^{2}H NMR experiments. The protein concentration used was 4 mol % for P-PLB or PLB with respect to lipids when conducting the ^{13}C CP-MAS NMR experiments.

Solid-State NMR Spectroscopy. A 500 MHz WB Bruker Avance solid-state NMR spectrometer and a Bruker 4 mm triple resonance CP-MAS probe (Bruker, Billerica, MA) were used to collect the ^{2}H, ^{31}P, and ^{13}C solid-state NMR spectra. For ^{2}H solid-state NMR experiments, the spectrometer was operated as 76.77 MHz, and the quadrupolar echo pulse sequence was employed using quadrature detection with complete phase cycling of the pulse pairs (*77*). The 90° pulse length was 3 μs, the inter-pulse delay was 40 μs, the recycle delay was 0.5 s, and the spectral width was set to 100 kHz. A total of 20 K transients were averaged for each ^{2}H solid-state NMR spectrum and processed using 300 Hz line broadening. ^{31}P NMR spectra were recorded with ^{1}H decoupling using a 4 μs $\pi/2$ pulse for ^{31}P and a 4 s recycle delay, 2 K scans were averaged, and the free induction decay was processed using 100 Hz of line broadening. The spectral width was set to 300 ppm. ^{31}P T_{1Z} longitudinal relaxation experiments were conducted using an inversion−recovery pulse sequence 180°-*T*-90°-acq with the sample spinning (4 kHz) at the magic angle. After the 180° pulse, the delay time (*T*) was varied from 10.0 ms to 6.0 s. The recycle delay was set to 10 s. In order to measure T_1, the change in the area under a particular peak was fitted to a single-exponential function: $I(t)=I(0) - A\exp(-t/T_1)$, where $I(0)$ is close to 1, and *A* is about 2 (*28*).

The ^{13}C CPMAS NMR experiments were performed at ^{1}H and ^{13}C resonance frequencies of 500.13 and 125.78 MHz, respectively. The ^{1}H 90° pulse length was 4.5 μs, the contact time was 3 ms, and the recycle delay was 4.5 s, and 8000 scans were signal averaged. The spinning speed was controlled at 6 kHz at a temperature of −25 °C. The spectral width was set to 50 ppm. All ^{13}C chemical shifts were referenced relative to tetramethylsilane (TMS) at 0 ppm. Simulations of the ^{13}C NMR spectra were carried out using the DMFIT software program (Supporting Information, Figure 1S) (*78*).

NMR Data Analysis. All of the powder-type ^{2}H NMR spectra of multilamellar dispersions of POPC-d_{31} were numerically deconvoluted (dePaked) using the algorithm of McCabe and Wassal (*79, 80*). These spectra were dePaked such that the bilayer normal was perpendicular with respect to the direction of the static magnetic field. Then, the quadrupolar splittings were directly measured from the dePaked spectra and converted into order parameters as described before (*26*, *27*). For numbering, the ^{2}H nuclei attached to the terminal methyl carbons were assigned carbon number 15. The remaining ^{2}H assignments were made in decreasing order along the phospholipid acyl chain. The quadrupolar splittings of the CD_3 methyl groups at the end of the acyl chains are the smallest and close to 0 kHz because they rotate at the fastest frequency. The second smallest splitting was assigned to the ^{2}H attached to C-14, and so forth along the acyl chain. The quadrupolar splittings for the deuterons in the plateau region were estimated by integration of the last broad peak. The order parameters calculated for the CD_3 quadrupolar splitting were multiplied by three according to procedures in the literature (*81*, *82*).

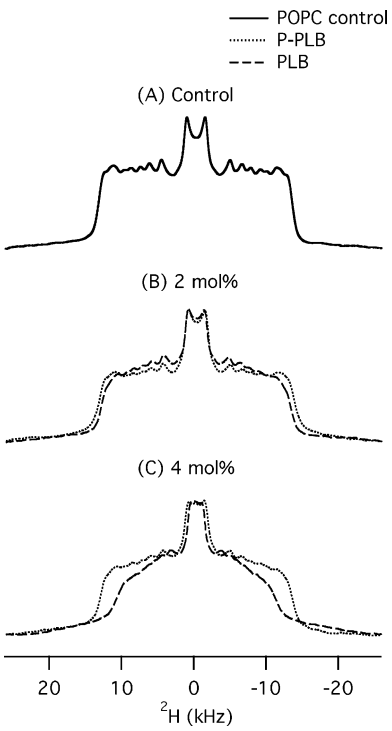

FIGURE 2: ^{2}H NMR powder-pattern spectra of the POPC bilayers in the absence (A, solid line) and presence of 2 mol % (B) and 4 mol % (C) PLB (dashed lines) and P-PLB (dotted lines) with respect to the lipids at 25 °C.

RESULTS

^{2}H NMR Study of PLB and P-PLB Incorporated into POPC Bilayers. The effect of PLB and P-PLB on the order and dynamics of the acyl chains of POPC-d_{31} bilayers was investigated utilizing ^{2}H solid-state NMR spectroscopy in the absence (Figure 2A) as well as in the presence of 2 mol % (Figure 2B) and 4 mol % (Figure 2C) PLB and P-PLB at 25 °C. In Figure 2(A), the central resonance doublet corresponds to the terminal CD_3 groups and the remaining overlapped doublets result from the different CD_2 segments of the acyl chain of POPC-d_{31}. The addition of 2 mol % and 4 mol % P-PLB to POPC MLVs slightly alters the ^{2}H NMR spectra (Figure 2B and C) compared to that of the control (Figure 2A) sample. Conversely, an inspection of Figure 2B and C clearly indicates that the addition of 2 mol % and 4 mol % PLB to the POPC-d_{31} bilayers significantly alters the line shape and the spectral resolution of the ^{2}H NMR spectra compared to that of the control (Figure 2A) sample. The loss in spectral resolution is manifested by the disappearance of the sharp edges of the ^{2}H peaks of 2 mol % and 4 mol % PLB in POPC bilayers. The changes in spectral resolution of the ^{2}H NMR spectra indicate that PLB interacts more significantly with the POPC-d_{31}-containing MLVs than with P-PLB.

Additionally, the effect of temperature increase (25−55 °C) on the order and dynamics of the acyl chains of POPC MLVs was investigated. The ^{2}H solid-state NMR spectra indicate that as the temperature increases, the quadrupolar splittings decrease for all samples with and without PLB and

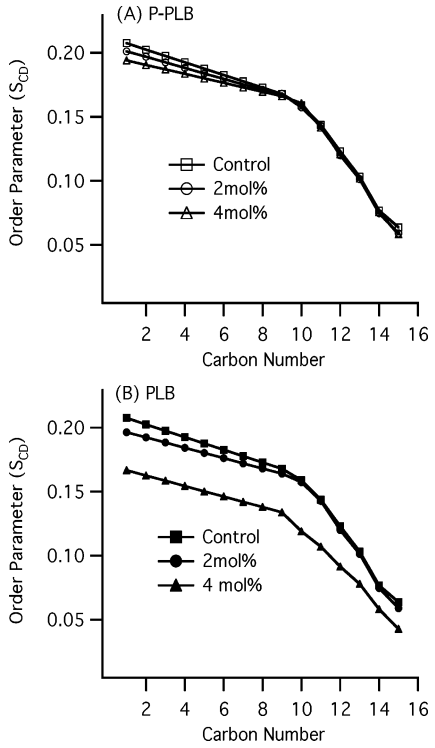

FIGURE 3: Smoothed acyl chains orientational order S_{CD} profiles calculated from the dePaked ^{2}H NMR spectra of Figure 2. The open squares, circles, and triangles (A) represent POPC bilayers with 0 mol %, 2 mol %, and 4 mol % P-PLB, respectively. The closed squares, circles and triangles (B) represent POPC bilayers with 0 mol %, 2 mol %, and 4 mol % PLB, respectively.

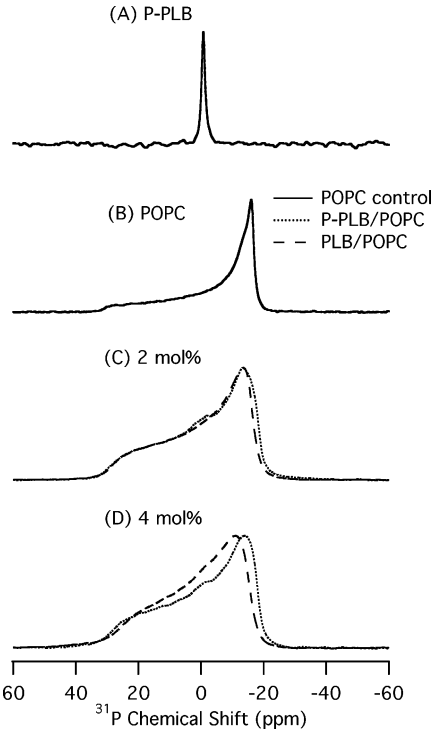

FIGURE 4: Static ^{31}P solid-state NMR spectrum of P-PLB without POPC lipids investigated at 25 °C (A, solid line). Static ^{31}P solid-state NMR spectra of POPC phospholipid in the absence (B, solid line) and presence of 2 mol % (C) and 4 mol % (D) P-PLB (dotted lines) and PLB (dashed lines) with respect to the POPC lipids investigated at 25 °C.

P-PLB, implying that the mobility of the acyl chains increases as the temperature increases (data not shown).

Figure 3 displays the smoothed segmental C−D bond order parameters (S_{CD}) of the POPC-d_{31} acyl chains calculated by dePakeing the corresponding ^{2}H NMR powder spectra shown in Figure 2. Figure 3A reveals a characteristic profile of decreasing order (S_{CD}) with increasing distance from the glycerol backbone for the pure bilayer as well as 2 mol % and 4 mol % P-PLB samples at 25 °C. In Figure 3A, there is a slight difference in the order parameter profile of POPC-d_{31}-containing bilayers in the presence of 2 mol % and 4 mol % of P-PLB compared to that of the control sample (without P-PLB). Conversely, for the PLB samples (Figure 3B), there is more disorder and motion in the acyl chain upon incorporation of 2 mol % and 4 mol % PLB when compared to that in the control sample (without PLB).

^{31}P NMR Studies of PLB and P-PLB Interacting with POPC MLVs. The static ^{31}P NMR spectrum of P-PLB protein dissolved in TFE in the absence of POPC lipids at 25 °C is shown in Figure 4 A. The isotropic peak corresponds to the phosphate group, attached to Ser16, of the dissolved P-PLB rotating fast in the absence of lipids. The static ^{31}P NMR spectra of POPC lipid bilayers prepared in the absence and presence of 2 mol % and 4 mol % of PLB and P-PLB at 25 °C are shown in Figure 4B, C, and D. At 25 °C, the motionally averaged powder pattern spectra are characteristic of MLVs in the liquid crystalline phase (L_α) and are expected for POPC bilayers at a temperature well above the chain melting point transition temperature (the T_m value is −2 °C for POPC) (*83*, *84*). The addition of PLB or P-PLB (Figure 4C and D) broadens the corresponding ^{31}P line shapes compared to that in pure POPC bilayers (Figure 4B). The chemical shift anisotropy (CSA) widths were measured for the pure POPC MLVs (Figure 4B), CSA = 48 ppm) as well as for the POPC MLVs interacting with 2 mol % P-PLB (Figure 4C), CSA = 46 ppm), 2 mol % PLB (Figure 4C), CSA = 45 ppm), 4 mol % P-PLB (Figure 4D), CSA = 45 ppm), and 4 mol % PLB (Figure 4D), CSA = 41 ppm). The measured CSA values are arranged (from high to low) in the following order: CSA control > P-PLB > PLB. Clearly, the ^{31}P line shape and CSA width data indicate that the POPC head groups are perturbed the most by the addition of 4 mol % PLB than by 4 mol % P-PLB (Figure 4D). These results agree with our ^{2}H solid-state NMR spectra described previously.

The powder pattern ^{31}P NMR spectra of POPC MLVs, with and without 4 mol % P-BLB and 4 mol % PLB, were recorded at temperatures ranging from 25 to 55 °C, and the chemical shift anisotropy (CSA) widths were measured (data not shown). The data indicate that as the temperature increases, the CSA of POPC bilayers (with and without PLB or P-PLB) decreases, indicating that the axial rotational motion of the phospholipid head groups increases with temperature.

In order to further probe the interaction of PLB with the phospholipid head groups, ^{31}P MAS T_1 relaxation experiments were conducted (Figure 5) (*28*). The ^{31}P T_1 spin−lattice relaxation rates are sensitive to the rapid conformational changes of lipid acyl chains and polar head groups as well as to changes in the long axis rotation and diffusion of lipids upon peptide interaction (*22*). Figure 5 indicates that the ^{31}P T_1 value of pure POPC MLVs increases as the temperature increases for temperatures ranging from 25 to

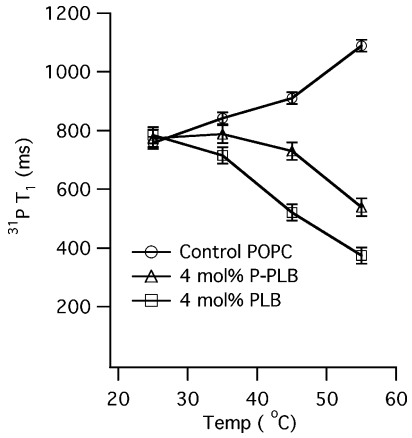

FIGURE 5: ^{31}P spin-lattice relaxation T_1 as a function of temperature (25−55 °C) of POPC phospholipid bilayers with and without 4 mol % protein with respect to the lipids. The open circles represent a POPC control (without protein) sample. The open triangles and squares represent POPC bilayers with 4 mol % P-PLB and PLB, respectively. The error bars were obtained by averaging ^{31}P T_1 values from two different sample sets.

55 °C. At 25 °C, there is no significant difference in the ^{31}P T_1 relaxation values among the 4 mol % P-PLB, 4 mol % PLB, and POPC control samples. However, Figure 5 reveals that the ^{31}P T_1 relaxation time of the 4 mol % P-PLB and PLB sample is considerably less than the POPC control at biologically relevant temperatures and above, ranging from 35 to 55 °C. Interestingly, the data indicates that this ^{31}P T_1 gap increases as the temperature increases. Additionally, the ^{31}P T_1 relaxation time difference between the control and the 4 mol % P-PLB sample is less than the difference between the control and the 4 mol % PLB sample. For example, at 35 °C, the ^{31}P T_1 differences between the control and both the 4 mol % P-PLB sample and the 4 mol % PLB sample are 60 and 140 ms, respectively. These results agree with the ^{31}P solid-state NMR powder spectra described previously, implying that PLB interacts more significantly with the head groups of the POPC bilayers than with its phosphorylated form (P-PLB).

^{13}C CP-MAS Solid-State NMR Spectroscopy on PLB and P-PLB. In order to probe the secondary structure of PLB and P-PLB in phospholipid bilayers, ^{13}C CPMAS solid-state NMR data were collected. The ^{13}C═O CPMAS solid-state NMR peak is very sensitive to the secondary structure of the protein (*30*, *32*, *85*). A ^{13}C═O CPMAS solid-state NMR peak between 174 and 177.5 ppm corresponds to an α-helical structure originating from the ^{13}C═O labeled residue of the protein (*30*, *32*, *85*). In addition, a ^{13}C═O CPMAS solid-state NMR peak at 172.4 ppm corresponds to either a β-sheet or an unstructured conformation of the peptide (*30*).

Figure 6 displays the ^{13}C-CPMAS solid-state NMR spectra of ^{13}C═O labeled Leu39-PLB (Figure 6A), Ala15-PLB (Figure 6B), and Ala15-P-PLB (Figure 6C) proteins upon insertion into POPC bilayers as well as the ^{13}C CPMAS solid-state NMR spectrum of the natural abundance carbonyl of pure POPC bilayers (Figure 6D) at −25 °C. All samples in Figure 6 were collected using the same lipid concentration and the same number of scans. A comparison of the first three spectra (Figure 6A, B, and C) with the control POPC spectrum (Figure 6D) indicates that the signal intensities of the ^{13}C═O labeled amino acid residues are considerably higher than the signal intensity of the background natural

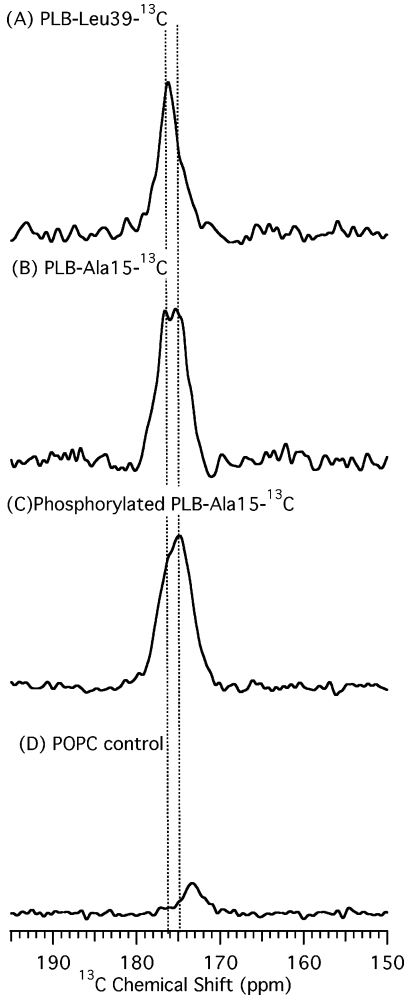

FIGURE 6: ^{13}C-CPMAS solid-state NMR spectra of ^{13}C═O labeled Leu39-PLB (A), Ala15-PLB (B), and Ala15-P-PLB (C), upon insertion into the POPC bilayers at −25 °C. At the same temperature (−25 °C), the ^{13}C-CPMAS solid-state NMR spectrum of the natural abundance ^{13}C carbonyl of POPC bilayers (without protein) is shown in (D).

abundance of the POPC ^{13}C carbonyl carbon of the control sample. Although it cannot be clearly seen because of low intensity, the natural abundance lipid's ^{13}C carbonyl carbon chemical shift of the first three spectra (Figure 6A, B, and C) is expected at about 174 ppm. The ^{13}C CPMAS solid-state NMR spectrum of ^{13}C═O labeled Leu39 residue (located within the transmembrane domain of PLB) reveals one well-resolved peak at 175.8 ppm (Figure 6A), indicating that Leu39 (transmembrane segment) is in an α-helical structural conformation. In Figure 6B, the ^{13}C NMR spectrum corresponding to the ^{13}C═O labeled Ala15 residue located within the cytosolic domain of PLB reveals 2 peaks with similar intensities at 176.5 and 175 ppm. These 2 peaks suggest that the cytoplasmic domain of PLB is in two different α-helical structural conformations. Similarly, in Figure 6C, the ^{13}C NMR spectrum corresponding to the ^{13}C═O labeled Ala15 residue located within the cytosolic domain of P-PLB reveals two peaks at 176 and 175 ppm. However, the intensities of these two peaks are unequal. All of the experimental spectra in Figure 6 were simulated and are shown in the Supporting Information (Figure 1S).

DISCUSSION

PLB Interacts with POPC Bilayers. The structure described by the Chou group of WT-PLB in micelles suggests that the cytoplasmic domain of the PLB pentamer is, on average, oriented away from the membrane surface, minimizing the possibility of its interaction with the head groups (*61*); however, the interaction of the full-length PLB pentamer with the MLVs' head groups from the lipid perspective utilizing solid-state NMR spectroscopy has not been reported in the literature. Only the interaction of the transmembrane and cytoplasmic domains of the AFA-PLB monomer or segmented portions of the WT-PLB pentamer (not the full-length pentamer) have been studied with the membrane (*27*, *58*, *59*, *62*). Therefore, three new solid-state NMR experiments were conducted, and the results indicate that the full-length WT-PLB interacts with POPC lipid bilayers. First, the molecular order parameter (S_{CD}) profiles of the ^{2}H solid-state NMR spectra indicate that PLB disturbs the order of the acyl chains of POPC-d_{31} doped MLVs. Additionally, the line shape and CSA of static ^{31}P solid-state NMR spectra of the POPC bilayers indicate that PLB strongly interacts with the head group region of the POPC MLVs. Finally, the dramatic changes observed in the ^{31}P T_1 values of PLB/POPC bilayers compared to those of the POPC control are obviously caused by PLB interacting with the head group region of the POPC bilayers. Similar changes in the ^{31}P T_1 values have been observed for complexes of cytochrome *c* interacting with DOPG and DOPS lipids (*86*).

In order to further investigate the effect of phosphorylation on the PLB pentamer upon interaction with the membrane, the same set of solid-state NMR spectroscopic experiments were conducted using the phosphorylated form of the PLB pentamer.

Comparing P-PLB and PLB Interacting with POPC Bilayers. The current ^{2}H and ^{31}P solid-state NMR data indicate that both PLB and P-PLB interact with POPC bilayers. However, the interaction of PLB with POPC MLVs is more significant compared that with phosphorylated PLB. The results indicate that the cytoplasmic domain of WT-PLB behaves in a manner similar to that of the AFA-PLB upon phosphorylation (*63*). Veglia and co-workers have indicated that phosphorylation of serine 16 (AFA-PLB) moves the cytoplasmic domain of AFA-PLB away from the lipid surface, and residues 15 and 16 of the cytoplasmic domain become part of the loop region (unstructured) upon phosphorylation (*63*). In order to further investigate the effect of phosphorylation on the secondary structure of the WT-PLB pentamer around the phosphorylation site, ^{13}C═O site-specific studies of PLB and P-PLB incorporated into lipid bilayers were conducted.

Secondary Structure of PLB and P-PLB in Phospholipid Bilayers. ^{13}C CPMAS NMR spectroscopy can be used to probe the secondary structure of WT-PLB and P-PLB proteins in POPC bilayers (*87*−*91*). The appearance of the single well-resolved peak at 175.8 ppm in the ^{13}C CPMAS solid-state NMR spectrum shown in Figure 6A indicates that Leu39 located in the transmembrane domain of PLB has one α-helical structural conformation. This agrees with all of the structural models shown in Figure 1.

Previous solid-state NMR spectroscopic studies have shown two peaks (176.8 and 172.4 ppm) in a similar environment for a ^{13}C═O-labeled Ala residue for the magainin antimicrobial peptide (see Table 1 for other examples) (*30*). In that magainin study, the first peak (176.8 ppm) was attributed to an α-helical structure, and the upfield peak at 172.4 ppm was attributed to either a *β*-sheet or an unstructured conformation of the peptide (*30*). This was confirmed by FTIR and additional NMR studies, which showed that the *β*-sheet magainin peptide rests on the outside of the lipid bilayer, whereas the α-helical portion must have been inserted inside the bilayer (*30*). Unlike magainin, in Figure 6B, which corresponds to the Ala15-PLB, two peaks at 176.5 and 175.3 ppm were observed. The two peaks are well within the range of an α-helical structure (Table 1). The observed α-helical structure of the cytoplasmic domain of PLB agrees with the L-shaped (Figure 1A) and bellflower-like assembly high-resolution solution NMR structures (Figure 1C) and disagrees with the non-α-helical disordered cytosolic domain model shown in Figure 1B (*57*, *60*, *61*).

Tuzi and co-workers have indicated that the local conformations of peptides and proteins can be characterized by examining the ^{13}C═O chemical shifts of the ^{13}C-labeled carbonyl of Ala, Leu, and Val and that chemical shifts may vary within the data range presented here for different conformational-dependent changes (*32*). Thomas and co-workers have probed the structural dynamics of the AFA-PLB monomer with a nitroxide spin label rigidly coupled to the peptide backbone utilizing EPR spectroscopy (*58*). They concluded that AFA-PLB is in a dynamic equilibrium between an ordered conformation that is in direct contact with the membrane surface and a dynamically disordered conformational state that is detached from the membrane and proposed to interact with the PLB regulatory target (*58*). In agreement with the two structural conformation models, the current ^{13}C solid-state NMR data of PLB-Ala15 (cytoplasmic domain) suggests that PLB incorporated within POPC bilayers has two different α-helical conformers.

Table 1: ^{13}C Carbonyl Chemical Shifts of Site-Specific Isotopically Labeled Proteins or Peptides and the Natural Abundance ^{13}C Chemical Shifts of the Carbonyl of Lipids

(A) Conformation-dependent ^{13}C═O chemical shifts of Ala residues

secondary structure	protein or peptide	^{13}C chemical shifts (ppm)	reference
α-helix	magainin analogue	176.8	Hirsh et al. (*30*)
	bacteriorhodopsin (Rb)	176.7	Kimura et al. (*31*)
	bacteriorhodopsin (Rb)	173.9−177.5	Tuzi et al. (*32*)
	polyalanine (PLA)	175.7−176.3	Lee et al. (*92*)
	polyalanine(PLA)	175.7−176.8	Henzler-Wildman et al. (*93*)
	Ala15-PLB	176.5 and 175.3	current study
	Ala15-P-PLB	176 and 175	current study
β-sheet	magainin analogue	172.4	Hirsh et al. (*30*)
	polyalanine (PLA)	172.1−173.1	Lee et al. (*92*)
	polyalanine (PLA)	171.6−173.1	Henzler-Wildman et al. (*93*)
	human calcitonin (hCT, residues 9−32)	173.1−173.7	Wagner et al. (*91*)
loop region	bacteriorhodopsin (Rb)	173.3−173.6	Tuzi et al. (*32*)

(B) Natural abundance ^{13}C chemical shift of the carbonyl of lipids

lipid	^{13}C chemical shifts (ppm)	reference
DMPC	173	Smith et al. (*85*)
egg PC	173.6	Yamaguchi et al. (*33*)
POPC	174	current study

Upon phosphorylation, Figure 6C, the ^{13}C NMR spectrum of P-PLB-Ala15 indicated one major peak at 175 ppm and a shoulder at 176 ppm. These observations suggest that the cytoplasmic domain of the Ala15-PLB pentamer, in its both phosphorylated and dephosphorylated states, is α-helical in structure around the phosphorylation site. This data agrees with the results previously reported by Arkin and co-workers (*42*). Their study indicates that phosphorylation does not significantly change the α-helical secondary structure of the WT-PLB in DMPC vesicles utilizing circular dichroism (CD) and Fourier transform infrared (FTIR) measurements (*42*).

Finally, in addition to its advantage in probing the secondary structure, ^{13}C CPMAS NMR spectroscopy can be used to demonstrate the absence of any nonspecific aggregation of WT-PLB and P-PLB proteins in POPC bilayers (*87*−*91*). ^{13}C CPMAS resonance peaks from unstructured protein/peptide aggregates are typically located near 172 ppm (*87*, *88*). The single well-resolved ^{13}C peak at 175.8 ppm shown in Figure 6A indicates that Leu39 located in the transmembrane domain of PLB has only one structural conformation that is α-helical. Furthermore, all three spectra in Figure 6A, B, and C (prepared under the same conditions) did not show any upfield peaks at 172 ppm, indicating that the they are homogeneous and fully hydrated and that the protein is properly folded and inserted (without any clusters or nonspecific aggregates) (*87*−*91*).

Mode of WT-PLB−*Membrane Interaction and the Protein's Physiological Function.* The new solid-state NMR spectroscopic data indicate that the interaction of PLB with the membrane surface significantly decreases upon phosphorylation. This finding agrees with results from the Simmerman group, in which phosphorylation of the WT-PLB pentamer shifts the cytoplasmic domain away from the lipid bilayer surface, decreasing the possibility of any interaction between the cytoplasmic domain and the membrane surface (*34*, *36*).

The model proposed by Chou's of WT-PLB interacting with SERCA assumes that it is possible for the pentameric form of PLB to initiate the binding of SERCA without even having to dissociate to the monomer, eliminating the energetic cost of the removal of a subunit (*61*). Additionally, they hypothesized that upon phosphorylation the introduced negative charge of the phosphate group at Ser16 or Thr17 could potentially alter the average orientation of the cytoplasmic domain of WT-PLB, leaving the helix less accessible to the calcium pump (*61*). Our results agree with Chou's hypothesis, which proposes a change in the orientation of the cytoplasmic domain upon phosphorylation.

Alternatively, our data fits very well with the concept of allosteric regulation previously proposed by the Veglia group for AFA-PLB (see the introduction for details) (*65*). When the WT-PLB is in its free form (not interacting with SERCA), the pentamer possibly interconverts between two populations (similar to the T-state and R-state of the AFA-PLB monomer). Simulations of Figure 6B and C (see Supporting Information, Figure 1S) suggest that phosphorylation shifts the population between the two proposed α-helical conformations from 50%:50% to 30%:70%. This observation could be explained in light of the ^{2}H and ^{31}P solid-state NMR data discussed previously. The predominant conformer (70%) of the P-PLB pentamer could have its cytoplasmic domain oriented away from the membrane surface, decreasing the P-PLB interaction with the membrane compared to that with unphosphorylated PLB. Finally, similar to the AFA-PLB mutant, we propose that the presence of SERCA could alter the distribution between the two WT-PLB populations observed in this study (*65*, *66*). Further experiments are needed to test this hypothesis.

CONCLUSION

This solid-state NMR spectroscopic study clearly shows membrane−protein interaction differences between PLB and P-PLB. From the perspective of the lipids, the ^{31}P and ^{2}H solid-state NMR spectroscopic data indicate that P-PLB has less direct contact with the membranes compared to that in WT-PLB. In addition, ^{13}C CP MAS solid-state NMR spectroscopy and $^{13}C{=}O$ site-specific (Ala15 residue) isotopically labeled proteins inserted into MLVs indicate that the PLB pentamer has two equally populated different α-helical structural conformations. However, upon phosphorylation, the conformer that possibly interacts less with the membrane becomes the predominant form. Finally, the data suggests that P-PLB conserves the α-helical structure of the Ala15 residue around the phosphorylation site (Ser 16) compared to that of PLB.

ACKNOWLEDGMENT

The authors thank Jun-Xia Lu for the help with the relaxation experiments.

SUPPORTING INFORMATION AVAILABLE

More details about the synthesis and purification of WT-PLB and P-PLB as well as the simulations of ^{13}C-CPMAS solid-state NMR spectra illustrated in Figure 6. This material is available free of charge via the Internet at http://pubs.acs.org.

REFERENCES

1. Arora, A., Abildgaard, F., Bushweller, J. H., and Tamm, L. K. (2002) NMR solution structure and dynamics of the outer membrane protein A transmembrane domain in dodecylphosphocholine micelles, *Biophys. J. 82*, 516A−516A.
2. Biverstahl, H., Andersson, A., Graslund, A., and Maler, L. (2004) NMR solution structure and membrane interaction of the N-terminal sequence (1-30) of the bovine prion protein, *Biochemistry 43*, 14940−14947.
3. Fernandez, C., and Wuthrich, K. (2003) NMR solution structure determination of membrane proteins reconstituted in detergent micelles, *FEBS Lett. 555*, 144−150.
4. Haugen, H. S., Fimland, G., Nissen-Meyer, J., and Kristiansen, P. E. (2005) Three-dimensional structure in lipid micelles of the pediocin-like antimicrobial peptide curvacin A, *Biochemistry 44*, 16149−16157.
5. Marcinowski, K. J., Shao, H., Clancy, E. L., and Zagorski, M. G. (1998) Solution structure model of residues 1-28 of the amyloid beta peptide when bound to micelles, *J. Am. Chem. Soc. 120*, 11082−11091.
6. Moberg, P., Nilsson, S., Stahl, A., Eriksson, A. C., Glaser, E., and Maler, L. (2004) NMR solution structure of the mitochondrial F-1 beta presequence from Nicotiana plumbaginifolia, *J. Mol. Biol. 336*, 1129−1140.
7. Papadopoulos, E., Oglecka, K., Maler, L., Jarvet, J., Wright, P. E., Dyson, H. J., and Graslund, A. (2006) NMR solution structure of the peptide fragment 1−30, derived from unprocessed mouse Doppel protein, in DHPC micelles, *Biochemistry 45*, 159−166.
8. Powers, J. P. S., Tan, A., Ramamoorthy, A., and Hancock, R. E. W. (2005) Solution structure and interaction of the antimicrobial polyphemusins with lipid membranes, *Biochemistry 44*, 15504−15513.

9. Watson, A. A., Fairlie, D. P., and Craik, D. J. (1998) Solution structure of methionine-oxidized amyloid beta-peptide (1-40). Does oxidation affect conformational switching? *Biochemistry 37*, 12700−12706.
10. Ying, J. F., Ahn, J. M., Jacobsen, N. E., Brown, M. F., and Hruby, V. J. (2003) NMR solution structure of the glucagon antagonist [desHis(1), desPhe(6), Glu(9)] glucagon amide in the presence of perdeuterated dodecylphosphocholine micelles, *Biochemistry 42*, 2825−2835.
11. Morrow, M. R., and Grant, C. W. M. (2000) The EGF-receptor transmembrane domain: peptide-peptide interactions in fluid bilayer membranes. *Biophys. J. 79*, 2024−2032.
12. Rigby, A. C., Barber, K. R., Shaw, G. S., and Grant, C. W. M. (1996) Transmembrane region of the epidermal growth factor receptor: Behavior and interactions via ^{2}H NMR, *Biochemistry 35*, 12591−12601.
13. Sharpe, S., Barber, K. R., Grant, C. W. M., Goodyear, D., and Morrow, M. R. (2002) Organization of model helical peptides in lipid bilayers: Insight into the behavior of single-span protein transmembrane domains, *Biophys. J. 83*, 345−358.
14. Sharpe, S., Barber, K. R., Grant, C. W. M., and Morrow, M. R. (2002) Evidence of a tendancy of self-association of the transmembrane domain of ErbB-2 in fluid phospholipid bilayers, *Biochemistry 41*, 2341−2352.
15. Yang, R., Yang, J., and Weliky, D. P. (2003) Synthesis, enhanced fusogenicity, and solid state NMR measurements of cross-linked HIV-1 fusion peptides, *Biochemistry 42*, 3527−3535.
16. Cross, T. A. (1997) Solid-state nuclear magnetic resonance characterization of gramicidin channel structure, *Methods Enzymol. 289*, 672−696.
17. Cross, T. A., and Opella, S. J. (1994) Solid-state NMR structural studies of peptides and proteins in membranes, *Curr. Opin. Struct. Biol. 4*, 574−81.
18. Long, J. R., Shaw, W. J., Stayton, P. S., and Drobny, G. P. (2001) Structure and dynamics of hydrated staherin on hydroxyapatite as determined by solid-state NMR, *Biochemistry 40*, 15451−15455.
19. Mani, R., Buffy, J. J., Waring, A. J., Lehrer, R. I., and Hong, M. (2004) Solid-state NMR investigation of the selective disruption of lipid membranes by protegrin-1, *Biochemistry 43*, 13839−13848.
20. Marcotte, I., Dufourc, E. J., Ouellet, M., and Auger, M. (2003) Interaction of the neuropeptide Met-Enkephalin with zwitterionic and negatively charged bicelles as viewed by ^{31}P and ^{2}H solid-state NMR, *Biophys. J. 85*, 328−339.
21. Nakazawa, Y., and Asakura, T. (2003) Structure determination of a peptide model of the repeated helical dmoain in Samia cynthia ricini silk fibroin before spinning by a combination of advanced solid-state NMR methods, *J. Am. Chem. Soc. 125*, 7230−7237.
22. Watts, A. (1998) Solid-state NMR approaches for studying the interaction of peptides and proteins with membranes, *Biochim. Biophys. Acta 1376*, 297−318.
23. Koenig, B. W., Ferritti, J. A., and Gawrisch, K. (1999) Site-specific deuterium order parameters and membrane-bound behavior of a peptide fragment from the intracellular domain of HIV-1 gp-41, *Biochemistry 38*, 6327−6334.
24. Laroche, G., Dufourc, E. J., Pezolet, M., and Dufourcq, J. (1990) Coupled changes between lipid order and polypeptide conformation at the membrane-surface: A ^{2}H NMR and raman-study of polylysine phosphatidic-acid systems, *Biochemistry 29*, 6460−6465.
25. Yamaguchi, S., Huster, D., Waring, A., Lehrer, R. I., Kearney, W., Tack, B. F., and Hong, M. (2001) Orientation and dynamics of an antimicrobial peptide in the lipid bilayer by solid-state NMR spectroscopy, *Biophys. J. 81*, 2203−2214.
26. Abu-Baker, S., Qi, X., Newstadt, J., and Lorigan, G. A. (2005) Structural changes in a binary mixed phospholipid bilayer of DOPG and DOPS upon Sap C interaction at acidic pH utilizing ^{31}P and ^{2}H solid-state NMR spectroscopy, *Biochim. Biophys. Acta 1717*, 58−66.
27. Dave, P. C., Tiburu, E. K., Damodaran, K., and Lorigan, G. A. (2004) ^{31}P and ^{2}H solid-state NMR spectroscopic studies of the transmembrane domain of the membrane-bound protein phospholamban, *Biophys. J. 86*, 1564−1573.
28. Lu, J., Damodaran, K., Blazyk, J., and Lorigan, G. A. (2005) Solid-state nuclear magnetic resonance relaxation studies of the interaction mechanism of antimicrobial peptides with phospholipid bilayer membranes, *Biochemistry 44*, 10208−10217.
29. Santos, J. S., Lee, D. K., and Ramamoorthy, A. (2004) Effects of antidepressants on the conformation of phospholipid headgroups studied by solid-state NMR, *Magn. Reson. Chem. 42*, 105−114.
30. Hirsh, D. J., Hammer, J., Maloy, W. L., Blazyk, J., and Schaefer, J. (1996) Secondary structure and location of a magainin analogue in synthetic phospholipid bilayers, *Biochemistry 35*, 12733−12741.
31. Kimura, S., Naito, A., Tuzi, S., and Saito, H. (2002) Dynamics and orientation of transmembrane peptide from bacteriorhodopsin incorporated into lipid bilayer as revealed by solid state ^{31}P and ^{13}C NMR spectroscopy, *Biopolymers 63*, 122−131.
32. Tuzi, S., Naito, A., and Saito, H. (1993) A high-resolusion solid-state 13C-NMR study on [1-13C]Ala and [3-13C]Ala and [1-13C]-Leu and Val-labelled bacteriorhodopsin: Conformation and dynamics of transmembrane helics, loops and termini, and hydration-induced conformational changes, *Eur. J. Biochem. 218*, 837−844.
33. Yamaguchi, S., Shimono, K., Sudo, Y., Tuzi, S., Naito, A., and Kamo, N. (2004) Conformation and dynamics of the [3-13C]Ala, [1-13C]Val-labeled truncated pharaonis transducer, pHtrII(1-159), as revealed by site-directed 13C solid-state NMR: Changes due to association with phoborhodopsin (sensory rhodopsin II), *Biophys. J. 86*, 3131−3140.
34. Simmerman, H. K., Collins, J. H., Theibert, J. L., Wegener, A. D., and Jones, L. R. (1986) Sequence analysis of phospholamban: identification of phosphorylation sites and two major structural domains, *J. Biol. Chem. 261*, 13333−13341.
35. Simmerman, H. K. B., Kobayashi, Y. M., Autry, J. M., and Jones, L. R. (1996) A leucine zipper stabilizes the pentameric membrane domain of phospholamban and forms a coiled-coil pore structure, *J. Biol. Chem. 271*, 5941−5946.
36. Simmerman, H. K. B., and Jones, L. R. (1998) Phospholamban: protein structure, mechanism of action, and role in cardiac function, *Physiol. Rev. 78*, 921−947.
37. James, P., Inui, M., Tada, M., Chiesi, M., and Carafoli, E. (1989) Nature and site of phospholamban regulation of the calcium pump of sarcoplasmic reticulum, *Nature 342*, 90−92.
38. Kirchberger, M. A., Tada, M., and Katz, A. M. (1975) Phospholamban a regulatory protein of the cardiac sarcoplasmic reticulum, *Recent Adv. Stud. Card. Struct. Metab. 5*, 103−115.
39. Lehnart, S. E., Wolfgang, S., Burkert, P., Prestle, J., Just, H., and Hasenfuss, G. (1998) Sarcoplasmic Reticulum Proteins in Heart Failure, in *Cardiac Sarcoplasmic Reticulum Function and Regulation of Contractility* (Johnson, R. G., Jr., and Kranias, E.G., Ed.) pp 220−230, New York Academy of Sciences, New York.
40. Adams, P. D., Arkin, I. T., Engelman, D. M., and Brunger, A. T. (1995) Computational searching and mutagenesis suggest a structure for the pentameric transmembrane domain of phospholamban, *Nat. Struct. Biol. 2*, 154−162.
41. Arkin, I. T., Adams, P. D., Brunger, A. T., Smith, S. O., and Engelman, D. M. (1997) Structural perspectives of phospholamban, a helical transmembrane pentamer, *Annu. Rev. Biophys. Biomol. Struct. 26*, 157−179.
42. Arkin, I. T., Rothman, M., Ludlam, C. F. C., Aimoto, S., Engelman, D. M., Rothschild, K. J., and Smith, S. O. (1995) Structural model of the phospholamban ion-channel complex in phospholipid-membranes, *J. Biol. Chem. 248*, 824−834.
43. Fuji, J., Ueno, A., Kitano, K., Tanaka, S., Kadoma, M., and Tada, M. (1987) Characterization of structural unit of phospholamban by amino acid sequencing and electropherotic analysis, *Biochim. Biophys. Res. Commn. 138*, 1044−1050.
44. Houndonougbo, Y., Kuczera, K., and Jas, G. S. (2005) Structure and dynamics of phospholamban in solution and in membrane bilayer: Computer simulations, *Biochemistry 44*, 1780−1792.
45. Hubbard, J. A., Maclachlan, L. K., Meenan, E., Salter, C. J., Reid, D. G., Lahouratate, P., Humphries, J., Stevens, N., Bell, D., Neville, W. A., Murray, K. J., and Darker, J. G. (1994) Conformation of the cytoplasmic domain of phospholamban by NMR and CD, *Mol. Membr. Biol. 11*, 263−269.
46. Hughes, E., Clayton, J. C., and Middleton, D. A. (2005) Probing the oligomeric state of phospholamban variants in phospholipid bilayers from solid-state NMR measurements of rotational diffusion rates, *Biochemistry 44*, 4055−4066.
47. Hughes, E., and Middleton, D. A. (2003) Solid-state NMR reveals structural changes in phospholamban accompanying the functional regulation of Ca^{2+}-ATPase, *J. Biol. Chem. 278*, 20835−20842.
48. Kovacs, R. J., Nelson, M. T., Simmerman, H. B. K., and Jones, L. R. (1988) Phospholamban forms calcium selective channels in lipid bilayers, *J. Biol. chem. 263*, 18364−18368.

49. Lamberth, S., Schmid, H., Muenchbach, M., Vorherr, T., Krebs, J., Carafoli, E., and Griesinger, C. (2000) NMR solution structure of phospholamban, *Helv. Chim. Acta 83*, 2141−2152.
50. Li, H. M., Cocco, M. J., Steitz, T. A., and Engelman, D. M. (2001) Conversion of phospholamban into a soluble pentameric helical bundle, *Biochemistry 40*, 6636−6645.
51. Li, J. H., Xiong, Y. J., Bigelow, D. J., and Squier, T. C. (2004) Phospholamban binds in a compact and ordered conformation to the Ca-ATPase, *Biochemistry 43*, 455−463.
52. Lockwood, N. A., Tu, R. S., Zhang, Z. W., Tirrell, M. V., Thomas, D. D., and Karim, C. B. (2003) Structure and function of integral membrane protein domains resolved by peptide-amphiphiles: Application to phospholamban, *Biopolymers 69*, 283−292.
53. Metcalfe, E. E., Zamoon, J., Thomas, D. D., and Veglia, G. (2004) H-1/N-15 heteronuclear NMR spectroscopy shows four dynamic domains for phospholamban reconstituted in dodecylphosphocholine micelles, *Biophys. J. 87*, 1205−1214.
54. Mueller, B., Hunter, G. W., Karim, C. B., and Thomas, D. D. (2003) FRET detection of Ca-ATPase and phospholamban interaction in membranes, *Biophys. J. 84*, 264A−264A.
55. Tatulian, S. A., Jones, L. R., Reddy, L. G., Stokes, D. L., and Tamm, L. K. (1995) Secondary structure and orientation of phospholamban reconstituted in supported bilayers from polarized attenuated total-reflection FTIR spectroscopy, *Biochemistry 34*, 4448−4456.
56. Zhang, X. M., Kimura, Y., and Inui, M. (2004) Effects of phospholipids on the oligomeric structure of phospholamban (PLN), a regulator of Ca2+-ATPase of cardiac sarcoplasmic reticulum (SR), *J. Pharm. Sci. 94*, 109P−109P.
57. Andronesi, C. A., Becker, S., Seidel, K., Heise, H., Young, H. S., and Baldus, M. (2005) Detemination of membrane protein structure and dynamics by magic-angle-spininng solid-state NMR spectroscopy, *J. Am. Chem. Soc. 127*, 12965−12974.
58. Karim, C. B., Kirby, T. L., Zhang, Z. W., Nesmelov, Y., and Thomas, D. D. (2004) Phospholamban structural dynamics in lipid bilayers probed by a spin label rigidly coupled to the peptide backbone, *Proc. Natl. Acad. Sci. U.S.A. 101*, 14437−14442.
59. Mascioni, A., Karim, C., Zamoon, J., Thomas, D. D., and Veglia, G. (2002) Solid-state NMR and rigid body molecular dynamics to determine domain orientations of monomeric phospholamban, *J. Am. Chem. Soc. 124*, 9392−9393.
60. Zamoon, J., Mascioni, A., Thomas, D. D., and Veglia, G. (2003) NMR solution structure and topological orientation of monomeric phospholamban in dodecylphosphocholine micelles, *Biophys. J. 85*, 2589−2598.
61. Oxenoid, K., and Chou, J. J. (2005) The structure of phospholamban pentamer reveals a channel-like architecture in membrane, *Proc. Natl. Acad. Sci. U.S.A. 102*, 10870−10875.
62. Clayton, J. C., Hughes, E., and Middleton, D. A. (2005) The cytoplasmic domains of phospholamban and phospholemman associate with phospholipid membrane surfaces, *Biochemsitry 44*, 17016−17026.
63. Metcalfe, E. E., Traaseth, N. J., and Veglia, G. (2005) Serine 16 phosphorylation induces an order-to disorder transition in the monomeric phospholamban, *Biochemistry 44*, 4386−4396.
64. Li, J., and Bigelow, D. J. (2003) Phosphorylation by cAMP-dependent protien kinase modulates the structural coupling between the transmembrane and cytosolic domains of phospholamban, *Biochemistry 42*, 10674−10682.
65. Zamoon, J., Nitu, F., Karim, C., Thomas, D. D., and Veglia, G. (2005) Mapping the interaction surface of a membrane protein: Unveiling the conformational switch of phospholamban in calcium pump regulation, *Proc. Natl. Acad. Sci U.S.A. 102*, 4747−4752.
66. Karim, C. B., Zhang, Z., Howard, E. C., Torgersen, K. D., and Thomas, D. D. (2006) Phosphorylation-dependent conformational switch in spin-labeled phospholamban bound to SERCA, *J. Mol. Biol. 358*, 1032−1040.
67. Fuji, J., Ueno, A., Kitano, K., Tanaka, S., Kadoma, M., and Tada, M. (1987) Complete complementary DNA-derived amino acid sequence of canine cardiac phospholamban, *J. Clin. Invest. 79*, 301−304.
68. Yao, Q., Bevan, J. L., Weaver, R. F., and Bigelow, D. J. (1996) Purification of porcine phospholamban expressed in Escherichia coli, *Protein Expression Purif. 8*, 463−468.
69. Collins, J. G., Kranias, E. G., Reeves, A. S., Bilezikjian, L. M., and Schwartz, A. (1981) Isolation of phospholamban and a second proteolipid component from canine cardiac sarcoplasmic reticulum, *Biochem. Biophys. Res. Commun. 99*, 796−803.
70. Mayer, E., McKenna, J. E., Garsky, V. M., Burke, C. J., Mach, H., Middaugh, C. R., Sardana, M., Smith, J. S., and Johnson, R. G., Jr. (1996) Biochemical and biophysical comparison of native and chemically synthesized phospholamban and a monomeric phospholamban, *J. Biol. Chem. 271*, 1669−1677.
71. Tiburu, E. K., Dave, P. C., Damodaran, K., and Lorigan, G. A. (2004) Investigating leucine side-chain dynamics and backbone conformations of phospholamban incorporated in phospholipid bilayers utilizing ^{2}H and ^{15}N solid-state NMR spectroscopy, *Biochemistry 43*, 13899−13909.
72. Derivatives for enhanced peptide synthesis, in *Novabiochem 2004/2005 Catalog*, pp 185−188.
73. Derivatives for phosphopeptide synthesis, in *Novabiochem 2004/2005 Catalog*, pp 192−194.
74. Simmerman, H. K. B., Lovelace, D. E., and Jones, L. R. (1989) Secondary structure of detergent-solubilized phospholamban, a phosphorylatable, oligomeric protein of cardiac sarcoplasmic reticulum, *Biochim. Biophys. Acta 997*, 322−329.
75. Hughes, E., Clayton, J. C., and Middleton, D. A. (2005) Probing the oligomeric state of phospholamban variants in phospholipid bilayers from solid-state NMR measurements of rotational diffusion rates, *Biochemistry 44*, 4405−4066.
76. Ying, W., Irvine, S. E., Beekman, R. A., Siminovitch, D. J., and Smith, S. O. (2000) Deuterium NMR reveals helix packing interactions in phospholamban, *J. Am. Chem. Soc. 122*, 11125−11128.
77. Davis, J. H., Jeffrey, K. R., Bloom, M., and Valic, M. I. (1976) Quadrupolar echo deuteron magnetic resonance spectroscopy in ordered hydrocarbon chains, *Chem. Phys. Lett. 42*, 390−394.
78. Massiot, D., Fayon, F., Capron, M., King, I., Le calve, S., Alonso, B., Durand, J. O., Bujoli, B., Gan, Z., and Hoatson, G. (2002) Modelling one- and two-dimensional solid-state NMR spectra, *Magn. Reson. Chem. 40*, 70−76.
79. McCabe, M. A., and Wassall, S. R. (1995) Fast-fourier-transform depaking, *J. Magn. Reson., Ser B 106*, 80−82.
80. McCabe, M. A., and Wassall, S. R. (1997) Rapid deconvolution of NMR powder spectra by weighted fast fourier transformation, *Solid State Nucl. Magn. Reson. 10*, 53−61.
81. Huster, D., Arnold, K., and Garwrisch, K. (1998) Influence of docosahexaenoic acid and cholesterol on lateral lipid organization, *Biochemistry 37*, 17299−17308.
82. Stockson, G. W., Polnaszek, C. F., Tulloch, A. P., Hasan, F., and Hasan, I. C. P. (1976) Molecular motion and order in single bilayer vesicles and multilamellar dispersions of egg lecithin and lecithin-cholesterol moxtures. A deuterium nuclear magnetic resonance study of specifically labeld lipids, *Biochemistry 15*, 954−966.
83. http://www.avantilipids.com/TechnicalInformation.html, accessed 5/14/2006.
84. Seelig, J. (1978) ^{31}P Nuclear magnetic resonance and the head group structure of phospholipids in membranes, *Biochim. Biophys. Acta 515*, 105−140.
85. Smith, S. O., Kawakami, T., Liu, W., Ziliox, M., and Aimoto, S. (2001) Helical structure of phospholamban in membrane bilayers, *J. Mol. Biol. 313*, 1139−1148.
86. Pinheiro, T. J. T., and Watts, A. (1994) Lipid specificity in the interaction of cytochrome-C with anionic phospholipid-bilayers revealed by solid-state ^{31}P NMR, *Biochemistry 33*, 2451−2458.
87. Karp, E. S., Tiburu, E. K., Abu-Baker, S., and Lorigan, G. A. (2006) The structural properties of the transmembrane segment of the integral membrane protein phospholamban utilizing ^{13}C CPMAS, ^{2}H, and REDOR solid-state NMR spectroscopy, *BBA-Biomembranes 1758*, 772−780.
88. de Planque, M. R. R., Rijkers, D. T. S., Fletcher, J. I., Liskamp, R. M. J., and Separovic, F. (2004) The α-M1 segment of the nicotinic acetylcholine receptor exhibits conformational flexability in a membrane environment, *Biochem. Biophys. Acta 1664*, 40−47.
89. Saito, H., Tsuchida, T., Ogawa, K., Arakawa, T., Yamaguchi, S., and Tuzi, S. (2002) Residue-specific millisecond to microsecond fluctuations in bacteriorhodopsin induced by distrupted and disorganized two-dimensional crystal lattice, through modified lipid-helix and helix-helix interactions, as revealed by ^{13}C NMR, *Biochem. Biophys. Acta 1565*, 97−106.
90. Tuzi, S., Naito, A., and Saito, H. (1994) ^{13}C NMR study on conformation and dynamics of the transmembrane a-helices, loop, and C-terminus of [3-^{13}C]Ala-labeled bacteriorhodopsin, *Biochemistry 33*, 15046−15052.
91. Wagner, K., Beck-Sickinger, A. G., and Huster, D. (2004) Structural investigation of a human calcitonin-derived carrier

peptide in a membrane environment by solid-state NMR, *Biochemistry 43*, 12459−12468.
92. Lee, D. K., and Ramamoorthy, A. (1999) Determination of the solid-state conformation of polyalanine using magic-angle spinning NMR spectroscopy, *J. Phys. Chem. B 103*, 271−275.
93. Henzler Wildman, K. A., Lee, D. K., and Ramamoorthy, A. (2002) Determination of α-helix and -sheet stability in the solid-state: A solid-state investigation of poly(L-alanine), *Biopolymers 64*, 246−254.
94. Koradi, R., Billeter, M., and Wuthrich, K. (1996) MOLMOL: A program for display and analysis of macromolecular structures, *J. Mol. Graphics 14*, 51−55.

BI0614028